Oxygen isotope composition of waters recorded in carbonates in strong clumped and oxygen isotopic disequilibrium

Caroline Thaler[1*], Amandine Katz[1], Magali Bonifacie[1], Bénédicte Ménez[1], Magali Ader[1]

[1] Université de Paris, Institut de physique du globe de Paris, CNRS, F-75005 Paris France

***corresponding author: Thaler.caroline@gmail.com**

Abstract. Paleoenvironmental reconstructions, which are mainly retrieved from oxygen isotope ($\delta^{18}O$) and clumped isotope (Δ_{47}) compositions of carbonate minerals, are compromised when carbonate crystallization occurs in isotopic disequilibrium. To date, knowledge of these common isotopic disequilibria, known as vital effects in biogenic carbonates, remains limited and the potential information recorded by $\delta^{18}O$ and Δ_{47} offsets from isotopic equilibrium values is largely overlooked. Additionally, in carbonates formed in isotopic equilibrium, the use of the carbonate $\delta^{18}O$ signature as a paleothermometer relies on our knowledge of the paleowaters' $\delta^{18}O$ value, which is often assumed. Here, we report the largest Δ_{47} offsets observed to date (as much as -0.270‰), measured on microbial carbonates, that are strongly linked to carbonate $\delta^{18}O$ offsets (-25‰) from equilibrium. These offsets are likely both related to the microorganism metabolic activity and yield identical erroneous temperature reconstructions. Unexpectedly, we show that the $\delta^{18}O$ value of the water in which carbonates precipitated, as well as the water-carbonate $\delta^{18}O$ fractionation dependence to temperature at equilibrium can be retrieved from these paired $\delta^{18}O$ and Δ_{47} disequilibrium values measured in carbonates. The possibility to retrieve the $\delta^{18}O$ value of paleowaters, sediments' interstitial waters or organisms' body water at the carbonate precipitation loci, even from carbonates formed in isotopic disequilibrium, opens

long-awaited research avenues for both paleoenvironmental reconstructions and biomineralization studies.

1 Introduction

Oxygen isotope composition ($\delta^{18}O$) paired with clumped isotope composition (Δ_{47}) of carbonate minerals is increasingly used for reconstructing paleoenvironmental or diagenetic conditions (Ghosh et al., 2006; Henkes et al., 2018; Mangenot et al., 2018 a and b). The $\delta^{18}O$ of carbonates depends on both the $\delta^{18}O$ value of the water in which the carbonate precipitated and the precipitation temperature (Urey et al., 1951). Its use to reconstruct paleoenvironments can be combined with the new carbonate C-O "clumped isotopes" abundance (Δ_{47}) thermometer which depends only on the carbonate precipitation temperature (Ghosh et al., 2006). By combining the Δ_{47} derived temperatures and the carbonate $\delta^{18}O$ value ($\delta^{18}O_{carbonate}$), the $\delta^{18}O$ value of the water ($\delta^{18}O_{water}$) in which the carbonate precipitated can be retrieved. However, this requires that solid carbonate and water reached isotopic equilibrium, which is often hard to prove. Conversely, carbonate precipitation in isotopic disequilibrium is commonly encountered (Affek et al., 2014; Loyd et al., 2016). Out of equilibrium $\delta^{18}O$ and Δ_{47} values are particularly known to occur in biogenic carbonates (Thiagarajan et al., 2011, Bajnai et al., 2018)– the most abundant carbonates in the sedimentary record. To date, the reasons for these isotopic disequilibria in carbonates remain largely under-constrained. While Δ_{47} compositions of carbonates seemed at first free of any biologically-driven or mineral-specific fractionation known to affect $\delta^{18}O_{carbonate}$ compositions (Eiler, 2011), recently identified disequilibrium Δ_{47} values (Saenger et al., 2012; Affek, 2013; Tang et al., 2014; Burgener et al., 2018) open new perspectives to unravel the mechanisms responsible for oxygen isotopic disequilibrium in carbonate minerals. Even though these vital effect identification do not prevent $\delta^{18}O$ and Δ_{47} tools to be powerful paleothermometer as empirical

calibrations taking vital effects into account allow temperature reconstructions, it has become crucial to determine if the $\delta^{18}O$ and Δ_{47} disequilibria observed in carbonates as diverse as those found in coral reefs (Saenger et al., 2012), brachiopods (Bajnai et al., 2018), microbialites and methane seep carbonates (Loyd et al., 2016), along with speleothems (Affek et al., 2014) could be explained by oxygen-isotope disequilibria occurring in dissolved inorganic carbon (DIC) involved in carbonate precipitation. In this case, $\delta^{18}O$ and Δ_{47} disequilibria in biogenic carbonates would record information, however unavailable yet, on the physiological characteristics of carbonate-forming organisms.

In previous experiments we produced microbial calcium carbonates (Millo et al., 2012; Thaler et al., 2017) that recorded the strongest oxygen isotope disequilibrium ever identified between DIC and precipitation water (*i.e.* -25‰ offset from $\delta^{18}O_{carbonate}$ equilibrium values). We used carbonic anhydrase (CA), an enzyme able to accelerate oxygen isotope equilibration between DIC and water *via* fast CO_2 hydration and HCO_3^- dehydration. When CA was added to the precipitation water, the carbonate oxygen isotope compositions reached equilibrium with the precipitation water (Thaler et al., 2017). Here, we build up on these experiments as they offer a unique opportunity to assess experimentally whether carbonates precipitated from DIC in disequilibrium with water also record Δ_{47} disequilibrium values, and the type of information that is actually carried by these paired disequilibria. We latter show how and to what extent this can be applied to previously published cases of oxygen isotopic offsets from equilibrium values in both biogenic and abiotic carbonates.

2 Material and Methods

2.1 Precipitation of microbial carbonates

Carbonates were precipitated at 30±0.1°C using the procedure detailed in Millo et al., (2012) and Thaler et al., (2017) and summarized hereafter. The precipitation solution (initial pH = 6.0) was composed of

ions added to Milli-Q® water (resistivity = 18 MΩ·cm) by dissolving salts in the following order: $MgSO_4 \cdot 7H_2O$ (16 mM), NaCl (80 mM), KCl (4 mM), urea (33.3 mM), $CaCl_2$ (40 mM). The aim was to mimic the ionic composition of a groundwater (Millo et al., 2012). In experiments with CA whose $\delta^{18}O$ results (but not the Δ_{47} ones) were recently published in Thaler et al., (2017), the precipitation solution was supplemented with CA at a concentration of 2 mg/L. The precipitation solution (with or without CA) was then mixed at a volumetric ratio of 1:1 with the ureolytic soil bacteria *Sporosarcina pasteurii* (Fig.1) suspended in Milli-Q® water, at a final optical density at 600 nm of 0.100±0.010. For this study, 16 gastight Exetainer® vials were filled with the precipitation solution without CA in order to sacrifice them at regular time intervals (*i.e.* 30, 60, 120, 180, 360 min and 24 h) and thus obtain information on the kinetics of the reaction, while reproducing the procedure followed for the experiment with CA (Thaler et al., 2017) consisting of 27 vials sacrificed every 10 to 30 min and after 24 h. The vials capped with rubber septa were filled up to the brim, *i.e.* without headspace, hence preventing any gaseous exchange with the atmosphere or headspace gases.

Ureolysis corresponds to two hydrolysis : (i) the hydrolysis of urea into ammonia (NH_3) and carbamate (H_2N-COOH) ($H_2N-CO-NH_2 + H_2O \rightarrow NH_3 + H_2N-COOH$), which is catalyzed by urease and is the rate limiting step, and (ii) the rapid and spontaneous hydrolysis of carbamate into ammonia and $CO_{2(aq)}$ ($H_2N-COOH + H_2O \rightarrow NH_3 + CO_{2(aq)} + H_2O$) (Krebs and Roughton, 1948; Matsuzaki et al., 2013) or into H_2CO_3 ($H_2N-COOH + H_2O \rightarrow NH_3 + H_2CO_3$) (Mobley and Hausinger, 1989; Krajewska, 2009).

Ureolysis completion was followed by evaluating the production of dissolved inorganic nitrogen (DIN = NH_3+NH_4^+). Determination of pH, DIN concentration and amount of precipitated carbonates (Fig. 2), as well as isotopic measurements, were performed for each vial to monitor their evolution as the ureolysis reaction progresses. The pH initially increased from 6.0 to 9.0 due to NH_3 production by ureolysis and consecutive alkalinization of the precipitation solution (Fig. 2a). The subsequent carbonate precipitation (Fig. 2b) lowered pH to 8.6 (without CA) and 8.5 (with CA) and was followed by a second pH increase

to 8.8 (without CA) and 8.7 (with CA) when carbonate precipitation stopped while ureolysis continued. At ureolysis completion, all the calcium initially present in solution (*i.e.* the limiting reagent) has precipitated whereas 35 to 45% of the DIC produced by ureolysis remained in solution. Carbonate precipitates, formed at the bottom and on the wall of the vials, were immediately rinsed with a few drops of pure ethanol in order to dehydrate bacteria and prevent further ureolysis, carbonate formation and/or dissolution–reprecipitation processes. Ethanol was then removed, and prior to their collection, carbonates were dried overnight at 40°C in the vials placed in a ventilated oven equipped with desiccating beads. The major part of the carbonates precipitated in this study was composed of calcite (Thaler et al., 2017) with minor amounts of aragonite (1 to 4%), vaterite (2 to 4%) and magnesian calcite with low Mg content ($Mg_{0.064}$,$Ca_{0.936}$)CO_3 (up to 8%) (Thaler et al., 2017).

All of the measured chemical parameters (pH, DIC, amount of solid carbonates, Ca^{2+} concentration, DIN) along with DIC and solid carbonate $\delta^{13}C$ behave similarly with or without active CA (Thaler et al., 2017). It was not possible to measure Δ_{47} for all the precipitated carbonates due to their low amount, particularly for the tubes sacrificed at the beginning of the experiments (Supplementary Table S1).

2.2 $\delta^{18}O$ and Δ_{47} measurements and associated uncertainties

All the isotopic analyses were made at Institut de physique du globe de Paris (IPGP, France). $\delta^{18}O$ analyses were performed on carbonate powders of ca. 2 mg with a continuous helium-flow isotope ratio mass spectrometer AP 2003 (Analytical Precision 2003, GV Instruments) coupled to a gas chromatograph column (GC-IRMS, Chrompac Column Type 99960), as described in Millo et al., (2012) and Thaler et al., (2017). External reproducibility on carbonate standards is ±0.1‰ (1SD) and represents the uncertainty assigned to $\delta^{18}O_{carbonate}$ data.

115 The analytical procedure used for clumped isotope Δ_{47} measurements is only briefly presented
116 here and detailed in Bonifacie et al., (2017). About 5 mg of carbonates were digested at 90°C during 20
117 min with 104% phosphoric acid H_3PO_4 in a common acid bath. The produced gaseous CO_2 was purified
118 with a manual vacuum line before introduction into a Thermo Scientific MAT 253 dual-inlet mass
119 spectrometer. Each purified CO_2 gas was analyzed for their abundance in isotopologues with m/z from
120 44 to 49 versus a working gas provided by Oztech Trading Corporation with $\delta^{13}C$ = -3.71‰ VPDB and
121 $\delta^{18}O$ = +24.67‰ VSMOW, as determined with the international reference material NBS19. One single
122 Δ_{47} measurement corresponds to 70 cycles of 26 s integration time each (total integration time = 1820 s).
123 Conventional $\delta^{18}O$ and $\delta^{13}C$ data were also acquired simultaneously to Δ_{47} measurements with this
124 instrument (Supplementary Tables S1 and S2). They are in excellent consistency with data obtained with
125 the continuous-flow method on smaller samples (Supplementary Table S1).

126 The Δ_{47} is calculated as a function of the stochastic distribution of the CO_2 isotopologues, as
127 follows:

128 $$\Delta_{47} = \left[\left(\frac{R^{47}_{measured}}{R^{47}_{stochastic}} - 1\right) - \left(\frac{R^{46}_{measured}}{R^{46}_{stochastic}} - 1\right) - \left(\frac{R^{45}_{measured}}{R^{45}_{stochastic}} - 1\right)\right] \times 1000 \quad (1),$$

129 where Δ_{47} is expressed in per mil (‰), and R^{47}, R^{46} and R^{45} are the abundance ratios of the masses 47,
130 46, 45 respectively, relative to the mass 44 ($^{12}C^{16}O^{16}O$). $R^{X}_{measured}$ are measured ratios of the CO_2 sample.
131 $R^{X}_{stochastic}$ are calculated from the measured 44, 45, 46 and 47 abundance ratios. The amount of
132 isotopologues of mass 47 (mainly $^{13}C^{18}O^{16}O$, but also $^{12}C^{17}O^{16}O$ and $^{13}C^{17}O^{17}O$) measured within the
133 CO_2 sample extracted from the acid digestion of the carbonates is linked to the amount of isotopologues
134 of mass 63 (mainly $^{13}C^{18}O^{16}O^{16}O$) within the reacted carbonate mineral (Guo et al., 2009). For the
135 correction from ^{17}O interferences we used the ^{17}O correction parameters from Brand et al., (2010), as
136 recently recommended (Daëron et al., 2016, Schauer et al., 2016). In order to transfer the obtained raw

Δ_{47} data into the absolute Carbon Dioxide Equilibrium Scale "CDES" ($\Delta_{47\ CDES90}$ being the Δ_{47} values of carbonates reacted within acid at 90°C), standards of CO_2 gases equilibrated at 25°C and 1000°C and with bulk isotopic compositions covering the range of measured carbonate samples (δ^{47} values between -50 and +24‰) were analyzed interspaced with unknown samples (typically 15 equilibrated CO_2 gas analyses by discrete session of analysis, 4 analytical sessions in total; Supplementary Table S5). For each analytical session, as recommended in Dennis et al., (2011), the Δ_{47} data were finally corrected with a fixed Equilibrated Gas Line slope (only slightly varying from 0.0048 to 0.0062 over our analytical sessions) and an Empirical Transfer Function (slopes varying from 1.0859 to 1.1344) based on the equilibrated CO_2 standards. Finally, the accuracy of our whole dataset and processing procedure was validated on carbonate reference material (*i.e.* IPGP-Carrara and 102-GC-AZ01), typically analyzed every 2 unknown samples (Supplementary Table S5). The Δ_{47} values obtained at IPGP over the course of this study are $\Delta_{47\ CDES90}$ = 0.316±0.020‰ (1SD, n = 16) for IPGP-Carrara and $\Delta_{47\ CDES90}$ = 0.620±0.010‰ (1SD, n = 18) for 102-GC-AZ01. Those values are indistinguishable from the values obtained at IPGP over four years of analyses on the same instrument (n >300) or previously reported by other laboratories (Daëron et al., 2016).

2.3 Temperature estimates and associated uncertainties

Apparent temperatures issued from oxygen isotope compositions were calculated based on the measured $\delta^{18}O_{carbonate}$ values of both the precipitated carbonate and the precipitation water in each experimental vial (Supplementary Table S1) and using the equation of oxygen isotopes' fractionation between calcite and water from Kim and O'Neil, (1997). Apparent temperatures issued from clumped isotope compositions were calculated from $\Delta_{47\ CDES90}$ data using the composite universal Δ_{47}-T calibration (Eq. 3 from Bonifacie et al., (2017) with T, the temperature). It is noteworthy that our main observations and

conclusions do not change if other calibrations to temperature are used for $\delta^{18}O$ and/or Δ_{47} (Kelson et al., 2017) (see also Supplementary Table S3). For both proxies, the uncertainties on temperature estimates reported here correspond to the standard deviation of the mean of replicated isotopic measurements of the same powder propagated in the calibration equation (but the actual errors on the calibration themselves are not considered). Note that the long-term external reproducibility on homogeneous calcite reference materials found in this study (*i.e.* ±0.020‰, 1SD) is used for samples with only one measurement or with 1SD lower than 0.020‰ (Supplementary Tables S1 and S5, Supplementary Discussion).

For the temperature (T) derived from the Δ_{47} data, we chose the calibration determined by Bonifacie et al., (2017) as it integrates a consequent number of data (n > 300), which statistical weight have been properly considered, and covers a wide temperature range (from 1 to 350°C), three characteristics that were recently shown by several teams as governing the precision on Δ_{47}-T calibration equations (Bonifacie et al., 2017; Kelson et al., 2017; Fernandez et al., 2017). Importantly, this calibration covers the high apparent temperature ranges reported here (i.e., low Δ_{47} values) allowing to avoid loss of precision/accuracy when extrapolating to temperature ranges that have not been experimentally investigated. Finally the Bonifacie et al. (2017) calibration has been checked independently with other methods (Mangenot et al., 2017, Dassié et al., 2018) on the range of temperatures (~30 to 96°C) where most of available calibrations are diverging and/or not well constrained. Indeed, these studies report excellent consistencies: i/ between T Δ_{47} and homogenization temperatures from fluid inclusion microthermometry (Mangenot et al., 2017), and ii/ between the $\delta^{18}O_{water}$ values directly measured in fluid inclusions by cavity ring down spectroscopy and those calculated from combined $T\Delta_{47}$ and $\delta^{18}O_{carbonate}$ of the host-mineral (Dassié et al., 2018). Thought we recognize that the normalization to carbonate standards presented in Bernasconi et al. (2018) might become commonly used by the community in the future (ie.

with the on-going inter-comparison Intercarb project), we preferred not to use this correction frame here because not enough of the four carbonate standards proposed by Bernasconi et al., 2018 were run together with our samples (n= 14 run in total of ETH1, ETH2, ETH3, ETH4 standards; Supplementary Table S5), and such normalization method will then introduce larger uncertainty than the normalization we performed with the large number of equilibrated gases ran daily together with our unknowns (n= 104 equilibrated gas; Supplementary Table S5 — Note also 33 secondary carbonate standards 102-GC-AZ01 and IPGP-Cararra, also ran in other IPGP studies and some other laboratories). Also remarkably, Δ_{47} obtained here on the four ETH carbonate standards are all systematically higher than values reported in Bernasconi et al., 2018 (Supplementary Table S4). Thought the reason of this positive offset is still unclear, it is noteworthy that positive offsets are also observed when compiling other recent published values (Supplementary Table S4; Daëron et al. 2016; Schauer et al., 2016; Fiebig et al., 2019).

3 Results and Discussion

3.1 Δ_{47} and $\delta^{18}O$ compositions of microbial carbonates can present strongly correlated vital effects

We performed Δ_{47} measurements on (i) microbial carbonates precipitated without CA by faithfully replicating the experiment detailed in Thaler et al., (2017) and (ii) microbial carbonates precipitated in the presence of CA remaining from these experiments. These calcium carbonates were precipitated as the result of microbially-driven hydrolysis of urea into DIC and ammonia (Millo et al., 2012). They constitute a reliable model for carbonate precipitation triggered by enzymatic production or transport of DIC, as it is the case for micro- and macro-skeletal carbonates common in the Phanerozoic, and for microbially-mediated carbonates since the Precambrian.

Without CA, the isotopic values of the very first carbonate precipitates present strong isotopic offsets from equilibrium values. The Δ_{47} offset to equilibrium starts down to -0.270‰ (the largest Δ_{47} offset ever measured in solid carbonates) and the offset to equilibrium reaches -24.7‰ for $\delta^{18}O_{carbonate}$ (Fig. 3 and Supplementary Table S1). Both Δ_{47} and $\delta^{18}O_{carbonate}$ absolute values then increase as ureolysis progresses, reducing offsets from equilibrium values to -0.179‰ for Δ_{47} and -15.7‰ for $\delta^{18}O_{carbonate}$. In the presence of CA, the trends observed for the Δ_{47} and $\delta^{18}O_{carbonate}$ values are similar but the offsets from equilibrium are drastically reduced (down to -0.027‰ for Δ_{47} and -1.4‰ for $\delta^{18}O_{carbonate}$ at the end of the experiment; Fig. 3), hence attesting for on-going isotopic equilibration of DIC with water by CA enzymatic activity prior to and during carbonate precipitation. The comparable behavior of Δ_{47} and $\delta^{18}O_{carbonate}$ values with respect to CA suggests that both disequilibria are inherited from the $\delta^{18}O$ and Δ_{47} signatures of the DIC generated by the biological activity.

3.2 Δ_{47} and $\delta^{18}O_{carbonate}$ disequilibrium originate from the metabolic production of DIC

Here, we discuss the potential processes known to generate $\delta^{18}O$ and Δ_{47} isotope fractionations during carbonate precipitation and we identify the main mechanism explaining our paired Δ_{47} and $\delta^{18}O_{carbonate}$ disequilibria. The relatively high precipitation rate (R) in our experiments (log R = -3.95 $mol \cdot m^{-2} \cdot s^{-1}$; (Thaler et al., 2017)) can only account for an oxygen kinetic isotope fractionation (KIF) of about 1 to 2‰ for $\delta^{18}O$ values (Watkins et al., 2013), while the oxygen isotope disequilibrium recorded in our carbonates reaches -24.7‰. Degassing of CO_2, known to fractionate DIC oxygen isotopes (Affek and Zaarur, 2014), can be ruled out as there is no gas phase in our experiments (see Material and Methods). Any potential kinetic fractionation due to DIC diffusion (Thiagarajan et al., 2011) is also unlikely as precipitation occurred on the bacterial DIC-producing cells, as highlighted by scanning electron microscopy showing bacterial cells trapped within and at the surface of carbonate crystals (Fig. 1).

Accordingly, the large offsets from equilibrium values observed for both Δ_{47} and $\delta^{18}O$ in our microbial carbonates can only result from (i) a KIF induced by CO_2 hydration/hydroxylation into HCO_3^- (but only if ureolysis produces CO_2 rather than H_2CO_3, which has not been established yet (Matsuzaki et al., 2013)) or (ii) a metabolic isotopic signature of the DIC produced by the bacteria, inherited from the initial isotopic composition of urea and/or due to a KIF introduced by the urease enzyme. CO_2 hydration/hydroxylation leads to the formation of HCO_3^-, with two oxygen atoms coming from CO_2 and the third one from H_2O (hydration) or OH^- (hydroxylation). The $\delta^{18}O_{HCO3-}$ value can then be estimated using a simple mass balance calculation (Létolle et al., 1990b; Usdowski et al., 1991). The newly formed HCO_3^- is depleted in ^{18}O compared to the reacting CO_2 because of the incorporation of oxygen coming from H_2O or OH^-, both depleted in ^{18}O relative to ^{16}O in contrast with CO_2 (Green and Taube, 1963;Beck et al., 2005). Such a low $\delta^{18}O_{HCO3-}$ value, several per mil lower than the equilibrium one, can then be preserved in the calcium carbonate if precipitation occurs shortly after CO_2 hydration/hydroxylation and before the full equilibration with water (Rollion-Bard et al., 2003). Regarding clumped isotopes, ab initio calculations predict that the fractionation associated with CO_2 hydration/hydroxylation increases the relative abundance of ^{13}C-^{18}O bonds, and thus the Δ_{47} value (Guo, Ms 2009). Even though this predicted fractionation trend has previously been used to explain several datasets for which CO_2 hydroxylation was assumed to occur prior to carbonate precipitation (Tripati et al., 2015; Spooner et al., 2016), such a tendency can only be validated using data acquired on carbonates for which CO_2 hydration/hydroxylation is demonstrated. This is the case of (i) hyperalkaline travertines (Falk et al., 2016) even though part of the reported kinetic isotope fractionation can be interpreted as resulting from CO_2 dissolution process (Clark et al., 1992) and (ii) two experimental samples (Tang et al., 2014) precipitated at high pH where CO_2 hydroxylation dominates. Both studies show, in agreement with the ab initio calculations (Guo, Ms 2009), higher Δ_{47} and lower $\delta^{18}O_{carbonate}$ values compared to

equilibrium. Thus, in a case where ureolysis would produce CO_2 in isotopic equilibrium with water, the Δ_{47} values affected by CO_2 hydration/hydroxylation recorded in calcium carbonates should be higher than the equilibrium value, while our microbial carbonates are showing Δ_{47} values lower than equilibrium. Thus, we conclude that our low Δ_{47} values measured in carbonates can only be explained by a metabolic source effect. In our case it corresponds to the ureolytic production of DIC, either directly as H_2CO_3 or as CO_2, with a Δ_{47} value low enough to compensate for any potentially succeeding increase due to the KIF associated with CO_2 hydration/hydroxylation. Nonetheless, the slow but continuous increase observed in our experiment without CA for both Δ_{47} and $\delta^{18}O_{carbonate}$ values more likely reflects ongoing equilibration of DIC oxygen isotopes with water at a slow rate.

Our results highlight that the isotope clumping proceeds continuously as C-O bonds are breaking and re-forming in the DIC, allowing oxygen isotopes (^{16}O, ^{17}O and ^{18}O) to be redistributed between H_2O, OH^-, H_2CO_3, HCO_3^- and CO_3^{2-} species *via* H_2O/OH^- -attachment to CO_2 and -detachment from HCO_3^-. In the experiment with CA, both Δ_{47} and $\delta^{18}O_{carbonate}$ reach simultaneously values close to equilibrium and without CA both Δ_{47} and $\delta^{18}O_{carbonate}$ values increase simultaneously. This coevolution corroborates former observations of comparable kinetics for clumped isotopes and $\delta^{18}O$ equilibration between DIC and water or CO_2 and water once $\delta^{13}C$ is equilibrated (Affek, 2013; Clog et al., 2015). This principle has been used to correct for disequilibrium fractionation factor in speleothems (Affek et al., 2008).

3.3 Erroneous yet comparable temperatures reconstructed from disequilibrium Δ_{47} and $\delta^{18}O$ values in carbonates

Apparent temperatures were calculated from disequilibrium Δ_{47} values obtained in the experiment without CA using the calibration of Bonifacie et al., (2017). Ranging from 198±21°C to 115±8°C (Fig.

4), they are at odds with the actual precipitation temperature of 30±1°C (see Methods). This shows that when carbonates precipitate from DIC in oxygen-isotope disequilibrium with water, the abundance of ^{13}C–^{18}O bonds in carbonates does not correlate with precipitation water temperature. Conversely, the temperatures reconstructed from the Δ_{47} values of carbonates precipitated in the presence of CA, ranging from 47±6°C to 39±2°C, are much closer to the actual precipitation temperature. Interestingly, the apparent temperatures reconstructed using Kim and O'Neil et al., (1997) calibration from the $\delta^{18}O_{carbonate}$ and $\delta^{18}O_{water}$ values of the same samples show comparable offsets from the actual temperature in both experiments without CA (from 218±2°C to 139±1°C) and with CA (from 39±1°C to 37±1°C) (Fig. 4). Practically, this implies that similar temperatures calculated from both carbonate Δ_{47} and $\delta^{18}O_{carbonate}$ values (in a case where the precipitation water $\delta^{18}O$ can be determined) can neither constitute evidence against O-isotope disequilibrium nor confirm that this is the true precipitation temperature.

3.4 Δ_{47} and $\delta^{18}O_{carbonate}$ paired disequilibria record the $\delta^{18}O$ of the water in which the carbonates precipitated

The fact that both Δ_{47} and $\delta^{18}O_{carbonate}$ values permit to calculate similarly evolving apparent temperatures along the (dis)equilibration profile recorded in carbonates as the experiment proceeds, indicates that the $\delta^{18}O_{carbonate}$, $\delta^{18}O_{water}$, Δ_{47}, and apparent temperature values are all together linked. In a Δ_{47} versus $\delta^{18}O_{carbonate}$ diagram, all of our data align, irrespectively of the fact that they are in strong isotopic disequilibrium or close to equilibrium (Fig. 5). Their alignment is fitted with what would be expected for equilibrium Δ_{47} and $\delta^{18}O_{carbonate}$ values of calcite precipitated at various temperatures from a water at a given $\delta^{18}O_{water}$ value. This $\delta^{18}O_{water}$ value can be calculated by combining for the same temperature, the equations of Δ_{47} and $\delta^{18}O_{carbonate}$ temperature calibrations from Kim and O'Neil, (1997) and Bonifacie et al., (2017), respectively (Eq. 2):

297 $$\delta^{18}O_{water} = \exp\left[-\frac{18.03}{\sqrt{\frac{0.0422\times10^{6}}{\Delta_{47\ CDES90}}-0.1126}} + 32.42\times10^{-3} + \ln(\delta^{18}O_{carbonate}+1000)\right] - 1000 \quad (2),$$

298 with $\delta^{18}O_{water}$ and $\delta^{18}O_{carbonate}$ values in the same isotopic referential (here VSMOW), and Δ_{47} values
299 reported into the absolute Carbon Dioxide Equilibrated Scale ($\Delta_{47\ CDES90}$). The calibration of Kim and
300 O'Neil, (1997) was preferred over more recent calibration equations (e.g. Watkins et al., 2013) because
301 it provides the best consistency for temperatures reconstructed from both the carbonate $\delta^{18}O$ and Δ_{47}
302 values at temperatures above 100°C. Note that Kim and O'Neil, (1997) and Bonifacie et al., (2017)
303 calibrations were developed independently, which prevents circular reasoning. Finally, as Kim and
304 O'Neil, (1997) is the most used calcite calibration to date, it also allows for a broader comparison with
305 previously published results.

306 Despite the fact that the data present a large range of offsets from equilibrium (Fig. 5), the mean
307 $\delta^{18}O_{water}$ value calculated using Eq. 2 for each combination of Δ_{47} and $\delta^{18}O_{carbonate}$ values measured for
308 our carbonates is -8.0±2.8‰ (1SD), indistinguishable (*i.e.* within errors) from the $\delta^{18}O_{water}$ values
309 measured in our experiments (-6.4±0.2‰ with CA and -6.8±0.2‰ without CA; Fig. 5). Note that such
310 precision in $\delta^{18}O_{water}$ values found in disequilibrium carbonates is remarkable considering that even for
311 equilibrium carbonates at isotopic equilibrium for <u>both</u> $\delta^{13}C$ and $\delta^{18}O$, $\delta^{18}O_{water}$ can only be retrieved
312 from paired Δ_{47} and $\delta^{18}O_{carbonate}$ values with a precision of ±1‰ at best (see Supplementary information).
313 This opens the promising opportunity to retrieve the $\delta^{18}O$ value of the water in which carbonates
314 precipitated out of equilibrium for both $\delta^{18}O_{carbonate}$ and Δ_{47}.

315 In order to evaluate the applicability of such an approach to other types of carbonates, Fig. 6
316 compiles disequilibrium paired $\delta^{18}O_{carbonate}$ and Δ_{47} data from two previously published experimental
317 studies (Tang et al., 2014; Staudigel et al., 2018). These studies were chosen to further evaluate the
318 relevancy of our $\delta^{18}O_{carbonate}$- Δ_{47} correlation because they are the only published dataset reporting full
319 sets of <u>*measured (rather than calculated)*</u> $\delta^{18}O_{water}$, $\delta^{18}O_{carbonate}$ and Δ_{47} values, with <u>*one or both proxies*</u>

320 *showing disequilibrium*, together with precipitation temperatures. A perfect knowledge (*i.e.*
321 measurements and not estimates) of these four parameters is mandatory here to adequately test whether
322 the use of our new $\delta^{18}O_{water}$ proxy could be generalized to a large diversity of carbonates. This thus
323 precludes plotting in Fig. 6 most published Δ_{47} studies on both natural and experimental samples, in
324 which $\delta^{18}O_{water}$ and/or temperature were not directly measured. These two datasets are also recent
325 enough to allow the conversion of their Δ_{47} values to the currently used normalization method (*i.e.* the
326 CDES absolute reference frame). It will then allow comparison with future studies, if measuring and
327 reporting all these four parameters together become the rule rather than the exception in Δ_{47} studies. Fig.
328 6a shows paired $\delta^{18}O_{carbonate}$ and Δ_{47} values of abiotic carbonates produced at 5, 25 and 40°C that are
329 known to be affected by KIF due to fast precipitation and for at least two of them by KIF due to CO_2
330 hydration/hydroxylation prior to precipitation (Tang et al., 2004). Except for these two carbonate
331 samples, the data align on a Δ_{47} versus $\delta^{18}O_{carbonate}$ covariation curve that cannot be explained solely by
332 temperature variation. As for our microbial carbonates obtained with or without CA, the average
333 calculated $\delta^{18}O_{water}$ (Eq. 2; -11.2±1.5‰) matches within error with the measured $\delta^{18}O_{water}$ (-9.6±0.2‰)
334 (Dietzel et al., 2009).

335 Fig. 6b shows paired $\delta^{18}O_{carbonate}$ and Δ_{47} values of abiotic carbonates that were precipitated
336 during an initial CO_2 degassing + equilibration phase followed by solely equilibration with water at 5,
337 15 and 25°C (Staudigel et al., 2018). During the latter equilibration phase, even though the carbonates
338 precipitated out of isotopic equilibrium, the paired $\delta^{18}O_{carbonate}$ and Δ_{47} values align on a covariation
339 curve of average calculated $\delta^{18}O_{water}$ value (Eq. 2; -3.0±1.1‰) close to the measured $\delta^{18}O_{water}$ (-0.65‰).
340 As a major outcome of this study, we thus anticipate that reliable $\delta^{18}O_{water}$ values of precipitation water
341 can be retrieved from carbonates presenting Δ_{47} and $\delta^{18}O_{carbonate}$ values in strong disequilibrium.

342 Some data presented in Fig. 6 also permit to evaluate the conditions of applicability of our
343 approach. In Fig. 6a, the two data points deviating from the Δ_{47} versus $\delta^{18}O_{carbonate}$ covariation curve
344 correspond to carbonates precipitated at pH ~10 and 5°C (while the others formed at pH and
345 temperatures ranging from 8.3 to 9 and 5 to 40°C, respectively) that have recorded a KIF due to CO_2
346 hydration/hydroxylation prior to precipitation (Tang et al., 2014). At pH=10, CO_2 reacts at 95% with
347 OH^- and at 5°C, DIC isotopic equilibration with water takes days. To a lesser extent, the KIF induced by
348 CO_2 hydroxylation seems also visible at pH= 9 (and 40°C) where CO_2 reacts at 82% with OH^- but DIC
349 isotopic equilibration with water at 40°C only takes about 15 hours. As previously detailed, the direction
350 of these isotopic offsets from equilibrium is compatible with ab initio calculations (Guo, Ms, 2009) and
351 can be intuitively understood as follows: in carbonates derived from CO_2 hydroxylation, the $R^X_{stochastic}$
352 term used for the Δ_{47} calculation (Eq. 1) should be strongly modified as the ^{18}O concentration in OH^- and
353 H_2O is lower than in CO_2 and the reaction does not add more ^{13}C than what is present in CO_2. This
354 might explain why in the case of disequilibria acquired through CO_2 hydroxylation, the correlation
355 between paired $\delta^{18}O$ and Δ_{47} disequilibria and the precipitation water $\delta^{18}O$ is not preserved and $\delta^{18}O_{water}$
356 cannot be reconstructed by the approach proposed here. The negative slope associated with this KIF on
357 the Δ_{47} and $\delta^{18}O_{carbonate}$ diagram (Fig. 6a) is nevertheless a good tool to identify CO_2 hydroxylation
358 reactions.
359 In Fig. 6b, during the CO_2 degassing phase of the precipitation experiment (Staudigel et al.,
360 2018), the data also deviate from the $\delta^{18}O$ versus Δ_{47} covariation curve. This behavior was interpreted by
361 the authors as a decoupling between Δ_{47} and $\delta^{18}O_{carbonate}$ values due to variable kinetics of ^{12}C-O and
362 ^{13}C-O bounding. A known difference in equilibration kinetics takes place between C and O isotopes in
363 the carbonate system as carbon isotopes equilibrate in seconds, while oxygen isotopes necessitate
364 minutes to hour to equilibrate among the different oxygen-bearing species (*i.e.* CO_2, HCO_3^-,CO_3^{2-},H_2O,

365 OH^-), depending on the pH, temperature and salinity of the solution (Zeebe and Wolf-Gladrow, 2001).
366 However, note that in that experiment, the carbon isotope compositions evolved for several hours as a
367 result of CO_2 degassing (Staudigel et al., 2018). We propose here that CO_2 degassing, because it affects
368 both C and O isotopes, modifies the $R^X_{stochastic}$ term (in Eq. 1), thus preventing Δ_{47} and $\delta^{18}O$ to vary with
369 the proportionality that allows to retrieve the $\delta^{18}O_{water}$ value on a Δ_{47} versus $\delta^{18}O$ covariation plot.
370 Hence, as for CO_2 hydroxylation, in case of a KIF induced by CO_2 degassing, $\delta^{18}O_{water}$ cannot be
371 reconstructed exclusively from disequilibrium $\delta^{18}O_{carbonate}$ and Δ_{47} values.

372 In summary, we conclude that mechanisms that can drastically change the $R^X_{stochastic}$ term in Δ_{47}
373 calculation (such as CO_2 hydroxylation and degassing) prevent $\delta^{18}O_{water}$ reconstructions from paired
374 disequilibrium Δ_{47} and $\delta^{18}O_{carbonate}$ values. Nevertheless, these mechanisms lead to peculiar types of
375 carbonates (*i.e.* speleothems that form in caves from CO_2 degassing, and travertine that form on lands
376 where fluids and gas escape from subsurface reservoirs for CO_2 hydroxylation) that represent only a
377 small fraction of all the carbonates existing on Earth. We hypothesize that ureolysis, which consists in
378 two successive steps of urea hydrolysis, an exchange reaction with the H_2O molecule from the aqueous
379 medium, might give a DIC whose $R^X_{stochastic}$ term in Δ_{47} calculation is already close to that of a DIC
380 under equilibration with the $\delta^{18}O_{water}$. This would explain why even our most extreme out of equilibrium
381 carbonates still fall close to the Δ_{47} versus $\delta^{18}O_{carbonate}$ covariation line corresponding to the real $\delta^{18}O_{water}$
382 value.

383

384 **3.5 Toward a better understanding of body water $\delta^{18}O$ in biomineralizing organisms**

385 The ability to reconstruct precipitation water $\delta^{18}O_{water}$ from disequilibrium Δ_{47} and $\delta^{18}O_{carbonate}$ values
386 further allows to examine the origin of the vital effect observed in organisms for which (i) CO_2
387 degassing and hydration/hydroxylation KIF can be ruled out, and (ii) only small $\delta^{13}C$ variations are

388 observed, thus preserving the $R^{X}_{stochastic}$ term in Δ_{47} calculation. We hypothesize that such an approach
389 could open perspectives to understand how Δ_{47} and $\delta^{18}O$ signals are affected by kinetic effects in most of
390 the biogenic carbonates, provided that CO_2 hydroxylation or degassing do not occur prior to carbonate
391 precipitation. This approach could thus be applied to the vast majority of sedimentary carbonates
392 (Milliman et al., 1993) and since deep time (*i.e.* microbialites, brachiopods, bryozoans, bivalves,
393 foraminifera, coccoliths), even when $\delta^{18}O_{carbonate}$ variations occur in the shell of the organism.
394 Additionally, the data presented here stand as an experimental demonstration that the mechanisms
395 controlling carbonate $\delta^{18}O$ equilibration with water (*i.e.* DIC equilibration with water) also control solid
396 carbonate Δ_{47} equilibrium (Watkins et al., 2015). This result can be used to recover information on
397 biomineralization mechanisms. For example, in recent coccolithophorid *Emiliana huxleyi* culture
398 experiments, the calcitic shell produced by the organism systematically yields a 2‰ positive $\delta^{18}O$ offset
399 from equilibrium values while their Δ_{47} values seem to faithfully record precipitation temperature (Katz
400 et al., 2017). These coccolithophorids were grown in waters with different $\delta^{18}O_{water}$ compositions (*i.e.*
401 measured at -6.14, -5.82 and 0.65‰ VSMOW, that are respectively seawater A, B and C in Fig. 6c).
402 Based on our results, which demonstrate that no $\delta^{18}O$ disequilibrium should be recorded in solid
403 carbonates if the associated Δ_{47} is at equilibrium, we can assume that the coccoliths precipitated at
404 oxygen-isotope equilibrium and calculate from Eq. 2 the actual $\delta^{18}O$ value of the water in which
405 precipitation took place (respectively shifted by 1.0±0.2‰, 2.1±0.4‰ and 1.1±0.7‰ towards more
406 positive values compared to the $\delta^{18}O_{water}$ value measured for the culture medium water; Fig. 6c). This
407 could reflect a biologically-driven difference between the $\delta^{18}O$ of body water at the precipitation site
408 inside *E. huxleyi* and the $\delta^{18}O$ of ambient water (*i.e.* the culture medium water). This hypothesis is
409 supported by what is known about intracellular precipitation of coccolith performed by
410 coccolithophorids: each coccolith forms from the accumulation of coccolithosomes, which are vesicles

411 containing up to a dozen of 7 nm spherical calcium-rich granular units (Outka and Williams, 1971).
412 Water in these ~100 nm vesicles can be considered as a finite reservoir whose isotopic composition
413 could be modified through isotopic exchange with a DIC affected by metabolic isotope fractionation.
414 Another mechanism that could increase the $\delta^{18}O$ value of a finite water reservoir by equilibrating it with
415 a comparable reservoir of DIC would be the introduction of DIC systematically as CO_2. As HCO_3^- and
416 CO_3^{2-} are enriched in ^{16}O in comparison to CO_2, the CO_2 conversion to HCO_3^- and CO_3^{2-} at equilibrium
417 before precipitation would pump ^{16}O from water.

418 In both case scenarios, a local change in water isotopic composition requires that the water
419 molecules turnover (*i.e.* external inputs) in these cellular organites is slow enough. Coccolithosomes are
420 subunits of the Golgi complex, which is a system of flat stacked vesicles concentrating a lot of
421 membranes in a small location (Outka and Williams, 1971). It is thus plausible that in a single celled
422 organism, living in seawater and performing intracellular biomineralization, specific osmolarity and
423 water circulation regulation mechanism are occurring. It is particularly plausible in the Golgi complex,
424 whose water content is isolated from seawater by several membranes. We thus suggest that inside
425 coccolithosomes, coccoliths precursors precipitate in equilibrium with the body water for oxygen
426 isotopes, but that the body water has a different $\delta^{18}O$ value than the seawater, which explains the
427 observed $\delta^{18}O$ apparent fractionation while their Δ_{47} composition reflects culture temperature (Katz et
428 al., 2017). It has already been highlighted through geochemical analysis of coccoliths, that
429 coccolithosomes water has altered pH (Liu et al., 2018) and ion concentrations (Hermoso et al., 2017) in
430 comparison to seawater. We hypothesize that the internal $\delta^{18}O$ water would thus be another parameter
431 controlled by the coccolithophore algae.

432

3.6 Ubiquity of the observed $\delta^{18}O_{carbonate}$- $\delta^{18}O_{water}$-Δ_{47}-temperature covariations in both equilibrium *and* disequilibrium carbonates

As shown above, in a Δ_{47} versus $\delta^{18}O_{carbonate}$ diagram, disequilibrium carbonates precipitated at fixed temperature plot on the theoretical line of equilibrium carbonates precipitated with a similar $\delta^{18}O_{water}$ but at a different temperature. This is illustrated in Fig. 7 where the three disequilibrium data series studied in this paper (Fig. 5 for this study and Figs. 6a and b for datasets from Tang et al., (2014) and Staudigel et al., (2018)) align with equilibrium data series. In other words, the values of the disequilibrium $1000\ln\alpha_{carbonate\text{-}water}$ for oxygen isotopes (with $\alpha = \frac{\delta^{18}O_{carbonate}+1000}{\delta^{18}O_{water}+1000}$) are similar to the equilibrium $1000\ln\alpha_{carbonate\text{-}water}$ for any given, and independently determined, apparent Δ_{47} temperature (Fig. 7). In details, our closest to equilibrium data recording low apparent temperatures match better the predicted equations from Coplen, (2007) and Watkins et al.,(2013), recently updated (Daëron et al., 2019). This latter calibration is based on carbonates from two caves where calcite precipitate extremely slowly and is thus assumed to have precipitated at equilibrium. Note that the use of these two cave samples for determining the dependence to temperature of the equilibrium $1000\ln\alpha_{carbonate\text{-}water}$ relies on the assumption that constant environmental conditions, including temperature in the two caves (7.9 and 33.7°C) and the $\delta^{18}O_{water}$ value of the precipitation water, prevailed over the whole period of carbonate precipitation (Coplen, 2007; Kluge et al., 2014). In Fig. 7, the disequilibrium data recording high apparent temperatures (above 100°C) match better the predicted equation of Kim and O'Neil, (1997). This $1000\ln\alpha_{carbonate\text{-}water}$ dependence to temperature was established on carbonates precipitated in the laboratory at well-known $\delta^{18}O_{water}$ and temperatures (from 10 to 40°C), but suspected to present a small KIF due to a high precipitation rate that lowers the value of the $1000\ln\alpha_{carbonate\text{-}water}$ (Watkins et al., 2013). Despite this, we used this equation to retrieve the $\delta^{18}O_{water}$ from our experimental carbonates, because most of them are associated with high apparent Δ_{47} temperatures. Coplen, (2007) or Watkins et

al., (2013) equations would have return 2‰ lower values (ca. -10±2‰ compared to -8±3‰ calculated with Kim and O'Neil (1997) equation). From our results, due to our experimental condition and the associated error in our dataset, it is not possible and not our intention to argue in favor of one of these calibrations. This however shows how crucial it is to improve knowledge on the equilibrium $1000\ln\alpha_{carbonate\text{-}water}$ at both high and low temperatures in order to improve the accuracy and precision of our new proxy for reconstructing the $\delta^{18}O_{water}$ from which carbonates, even disequilibrium ones, precipitated.

Importantly, we here establish a new method to determine the equilibrium $1000\ln\alpha_{carbonate\text{-}water}$, which consists in using the kinetics of Δ_{47} and $\delta^{18}O$ covariations during (dis)equilibration. Notably, because of the very large range of apparent temperatures recorded by disequilibrium carbonates (between ~40 and 200°C; Fig. 7) this method could be particularly adapted to calibrate $1000\ln\alpha_{carbonate\text{-}water}$ at high temperatures for which the differences between the two most popular $1000\ln\alpha_{carbonate\text{-}water}$ dependence to temperature equations (Kim and O'Neil, 1997; Coplen, 2007) appear larger (Fig. 7). Unfortunately, none of the three experimental setups having produced these disequilibrium carbonates (this study, as well as Tang et al., 2014 and Staudigel et al., 2018) were designed for the purpose of calibrating the equilibrium $1000\ln\alpha_{carbonate\text{-}water}$. It is thus not possible using these datasets to propose a meaningful calibration. At least in our experiment, too many phenomena including the relatively high precipitation rate, variations in $\delta^{13}C$ values (~3‰) (Thaler et al., 2017), and the presence of traces of aragonite and vaterite in our carbonates (Supplementary Information) lower the accuracy of the reconstructed equilibrium $1000\ln\alpha_{carbonate\text{-}water}$ values.

As a broader perspective, we anticipate that such an approach will help in determining critical equilibrium fractionation factors for other gaseous isotopic systems (such as isotopologues of molecules containing S-O bounds) or minerals of prime interest in biology and geology if clumped isotopes

479 measurements expand further beyond gaseous mass spectrometry (*e.g.* bounding between Fe-O, Fe-S,
480 Ca-C).
481
482 **4. Conclusions**
483 Our experimental results show that the information held in disequilibrium (and apparent disequilibrium)
484 carbonates is diverse and promising. First, a paired Δ_{47} and $\delta^{18}O_{carbonate}$ disequilibrium indicates that
485 carbonates have precipitated in a dynamic environment where DIC and water did not reach isotopic
486 equilibrium. In our microbial carbonate experiments, all the DIC is produced in isotopic disequilibrium
487 with water and precipitates rapidly. Accordingly, the disequilibrium O isotope compositions recorded in
488 those carbonates are maximized compared to what can be expected in nature where newly produced DIC
489 is expected to be mixed with at least partly equilibrated ambient DIC before carbonates precipitate.
490 Second, the combined use of clumped and traditional oxygen isotopic compositions allows retrieving the
491 $\delta^{18}O$ of the precipitation water, *i.e.* organism body water or environmental water, even for carbonates
492 presenting $\delta^{18}O$ and/or Δ_{47} disequilibria or apparent disequilibria. Hence, except in the case of processes
493 such as CO_2 degassing and CO_2 hydration/hydroxylation, which likely modify the $R^X_{stochastic}$ term in Δ_{47}
494 calculation, paired Δ_{47} and $\delta^{18}O_{carbonates}$ disequilibria in carbonates can be used to reconstruct the
495 oxygen-isotope composition of both DIC and water at the precipitation loci even when precipitation
496 occurred under disequilibrium conditions. Third, the (dis)equilibration trend in a Δ_{47} versus $\delta^{18}O_{carbonates}$
497 covariation diagram can be used as a new method to determine the equilibrium fractionation factor
498 between carbonate and water for a wide range of temperatures. Altogether, this open up new avenues to
499 better constrain not only past climate changes through improved paleoenvironmental reconstructions but
500 also the physiology and habitat of sea-life sensitive to ocean acidification.
501

Data availability. All the data generated and analyzed in this study are available within the paper and in its Supplementary Information.

Author contributions

C.T. and A.K. conceived the research. C.T. performed the microbial precipitation experiment and the $\delta^{13}C$ and $\delta^{18}O$ analyses during her PhD thesis under M.A. and B.M. supervision. A.K. performed the Δ_{47} analyses during her PhD thesis under M.B. supervision. C.T. took the lead in the interpretation of the results and the writing of the original draft. All authors provided critical feedback and helped shaping the research, analyses and manuscript.

Competing interests The authors declare no competing financial interests.

Acknowledgements

This research was supported by French MRT PhD fellowships to C.T. and A.K., the Centre de Recherches sur le Stockage Géologique du CO_2 (IPGP-TOTAL-Schlumberger-ADEME) (B.M. and M.A.) and an Emergence grant from the Paris council to M.B. This study contributes to the IdEx Université de Paris ANR-18-IDEX-0001.

References

Affek, P. A., Bar-Matthews, M., Ayalon, A., Matthews, A. & Eiler, J. M.: Glacial/interglacial temperature variations in Soreq cave speleothems as recorded by "clumped isotope" thermometry. *Geochim. Cosmochim. Acta* **72**, 5351–5360, https://doi.org/10.1016/j.gca.2008.06.031, 2008.

524 Affek, H. P.: Clumped isotopic equilibrium and the rate of isotope exchange between CO_2 and
525 water. *Am. J. Sci.* **313**, 309–325, doi: 10.2475/04.2013.02, 2013.
526 Affek, H. P. Matthews, A., Ayalon, A., Bar-Matthews, M., Burstyn, Y., Zaarur, S., & Zilberman, T.:
527 Accounting for kinetic isotope effects in Soreq Cave (Israel) speleothems. *Geochim. Cosmochim.*
528 *Acta* **143**, 303–318, https://doi.org/10.1016/j.gca.2014.08.008, 2014.
529 Affek, H. P. & Zaarur, S.: Kinetic isotope effect in CO_2 degassing: Insight from clumped and oxygen
530 isotopes in laboratory precipitation experiments. *Geochim. Cosmochim. Acta* **143**, 319–330,
531 https://doi.org/10.1016/j.gca.2014.08.005, 2014.
532 Bajnai, D., Fiebig, J., Tomašových, A., Garcia, S. M., Rollion-Bard, C., Raddatz, J., Löffler, N.,Primo-
533 Ramos, C. & Brand, U.: Assessing kinetic fractionation in brachiopod calcite using clumped
534 isotopes. *Sci. Rep.* **8**, 533, https://doi.org/10.1038/s41598-017-17353-7, 2018.
535 Beck, W. C., Grossman, E. L. & Morse, J. W.: Experimental studies of oxygen isotope fractionation in
536 the carbonic acid system at 15, 25, and 40 °C. *Geochim. Cosmochim. Acta* **69**, 3493–3503,
537 https://doi.org/10.1016/j.gca.2005.02.003, 2005.
538 Bernasconi, S. M., Müller, I. A., Bergmann, K. D., Breitenbach, S. F., Fernandez, A., Hodell, D. A.,
539 Jaggi, M., Meckler, A. N., Millan, I., & Ziegler, M. Reducing uncertainties in carbonate clumped
540 isotope analysis through consistent carbonate-based standardization. *Geochem. Geophy. Geosy.* **19**,
541 2895-2914, https://doi.org/10.1029/2017GC007385, 2018.
542 Bonifacie, M. Calmels, D., Eiler, J. M., Horita, J., Chaduteau, C., Vasconcelos, C., Agrinier, P., Katz,
543 A., Passey, B. H., Ferry, J. M., & Bourrand, J. J..: Calibration of the dolomite clumped isotope
544 thermometer from 25 to 350° C, and implications for a universal calibration for all (Ca, Mg, Fe)CO_3
545 carbonates. *Geochim. Cosmochim. Acta* **200**, 255–279, https://doi.org/10.1016/j.gca.2016.11.028,
546 2017.

Brand, W. A., Assonov, S. S. & Coplen, T. B.: Correction for the ^{17}O interference in $\delta^{13}C$ measurements when analyzing CO_2 with stable isotope mass spectrometry (IUPAC Technical Report). *Pure Appl. Chem.* **82**, 1719–1733, https://doi.org/10.1351/PAC-REP-09-01-05, 2010.

Burgener, L. K., Huntington, K. W., Sletten, R., Watkins, J. M., Quade, J., & Hallet, B.: Clumped isotope constraints on equilibrium carbonate formation and kinetic isotope effects in freezing soils. *Geochim. Cosmochim. Acta* **235**, 402–430, https://doi.org/10.1016/j.gca.2018.06.006, 2018.

Clark, I. D., Fontes, J. C. & Fritz, P.: Stable isotope disequilibria in travertine from high pH waters: laboratory investigations and field observations from Oman. *Geochim. Cosmochim. Acta* **56**, 2041-2050, https://doi.org/10.1016/0016-7037(92)90328-G, 1992.

Clog, M., Stolper, D. & Eiler, J. M.: Kinetics of CO_2 (g)–H_2O (1) isotopic exchange, including mass 47 isotopologues. *Chem. Geol.* **395**, 1–10, https://doi.org/10.1016/j.chemgeo.2014.11.023, 2015.

Coplen, T. B.: Calibration of the calcite–water oxygen-isotope geothermometer at Devils Hole, Nevada, a natural laboratory. *Geochim. Cosmochim. Acta* **71**, 3948–3957, https://doi.org/10.1016/j.gca.2007.05.028, 2007.

Daëron, M., Blamart, D., Peral, M. & Affek, H. P.: Absolute isotopic abundance ratios and the accuracy of Δ_{47} measurements. *Chem. Geol*. **442**, 83–96, https://doi.org/10.1016/j.chemgeo.2016.08.014, 2016.

Daëron, M., Drysdale, R. N., Peral, M., Huyghe, D., Blamart, D., Coplen, T. B., Lartaud, F. & Zanchetta, G.: Most Earth-surface calcites precipitate out of isotopic equilibrium. *Nat. Commun.* **10**, 429, https://doi.org/10.1038/s41467-019-08336-5, 2019.

Dassié E. Genty, D., Noret, A., Mangenot, X., Massault, M., Lebas, N., Duhamel, M., Bonifacie, M., Gasparrini, M., Minster B., and Michelot, J.L.**:** A newly designed analytical line to examine the

reproducibility of fluid inclusion isotopic compositions in small carbonate samples. *Geochem. Geophy. Geosy.* **19**, 1107-1122. https://doi.org/10.1002/2017GC007289, 2018.

Dennis, K. J., Affek, H. P. & Schrag, D.: Defining an absolute reference frame for 'clumped' isotope studies of CO_2. *Geochim. Cosmochim. Acta* **75**, 7117–7131, https://doi.org/10.1016/j.gca.2011.09.025, 2011.

Dietzel, M., Tang, J., Leis, A. & Köhler, S. J.: Oxygen isotopic fractionation during inorganic calcite precipitation—Effects of temperature, precipitation rate and pH. *Chem. Geol.* **268**, 107–115 , https://doi.org/10.1016/j.chemgeo.2009.07.015, 2009.

Eiler, J. M.: Paleoclimate reconstruction using carbonate clumped isotope thermometry. *Quat. Sci. Rev.* **30**, 3575–3588, https://doi.org/10.1016/j.quascirev.2011.09.001, 2011.

Falk, E. S., Guo, W., Paukert, A. N., Matter, J. M., Mervine, E. M. & Kelemen, P. B.: Controls on the stable isotope compositions of travertine from hyperalkaline springs in Oman: Insights from clumped isotope measurements. *Geochim. Cosmochim. Acta* **192**, 1-28, https://doi.org/10.1016/j.gca.2016.06.026, 2016.

Fernandez, A., Müller, I. A., Rodríguez-Sanz, L., van Dijk, J., Looser, N., & Bernasconi, S. M.. A reassessment of the precision of carbonate clumped isotope measurements: Implications for calibrations and paleoclimate reconstructions. *Geochem., Geophy., Geosystems* **18**, 4375–4386, https://doi.org/10.1002/2017GC007106, 2017.

Fiebig, J., Bajnai, D., Löffler, N., Methner, K., Krsnik, E., Mulch, A., & Hofmann, S. Combined high-precision Δ48 and Δ47 analysis of carbonates. *Chem. Geol*., **522**, 186-191, https://doi.org/10.1016/j.chemgeo.2019.05.019, 2019.

590 Ghosh, P., Adkins, J., Affek H., Balta B., Guo W., Schauble E., Schrag D., & Eiler J.: $^{13}C–^{18}O$ bonds in
591 carbonate minerals: a new kind of paleothermometer. *Geochim. Cosmochim. Acta* **70**, 1439–1456,
592 https://doi.org/10.1016/j.gca.2005.11.014, 2006.
593 Green, M. & Taube, H.: Isotopic fractionation in the OH–H_2O exchange reaction. *J. Phys. Chem.* **67**,
594 1565–1566, https://doi.org/10.1021/j100801a507, 1963.
595 Guo, W. Carbonate clumped isotope thermometry: application to carbonaceous chondrites and effects of
596 kinetic isotope fractionation. Ph. D. thesis, California Institute of Technology, 261 p. (2009).
597 Guo, W., Mosenfelder, J. L., Goddard, W. A. III & Eiler, J. M.: Isotopic fractionations associated with
598 phosphoric acid digestion of carbonate minerals: insights from first principles theoretical modeling
599 and clumped isotope measurements. *Geochim. Cosmichim. Acta* **73**, 7203–7225,
600 https://doi.org/10.1016/j.gca.2009.05.071, 2009.
601 Henkes, G. A. Passey, B. H., Grossman, E. L., Shenton, B. J., Yancey, T. E., & Pérez-Huerta, A.:
602 Temperature evolution and the oxygen isotope composition of Phanerozoic oceans from carbonate
603 clumped isotope thermometry. *Earth Planet. Sci. Lett.* **490**, 40–50,
604 https://doi.org/10.1016/j.epsl.2018.02.001, 2018.
605 Hermoso, M., Lefeuvre, B., Minoletti, F., de Rafélis, M.: Extreme strontium concentrations reveal
606 specific biomineralization pathways in certain coccolithophores with implications for the Sr/Ca
607 paleoproductivity proxy. *PLoS ONE* **12**, e0185655, https://doi.org/10.1371/journal.pone.0185655,
608 2017.
609 Katz, A., Bonifacie, M., Hermoso, M., Cartigny, P. & Calmels, D.: Laboratory-grown coccoliths exhibit
610 no vital effect in clumped isotope (Δ_{47}) composition on a range of geologically relevant
611 temperatures. *Geochim. Cosmochim. Acta* **208**, 335–353, https://doi.org/10.1016/j.gca.2017.02.025,
612 2017.

613 Kelson, J. R., Huntington, K. W., Schauer, A. J., Saenger, C. & Lechler, A. R.: Toward a universal
614 carbonate clumped isotope calibration: Diverse synthesis and preparatory methods suggest a single
615 temperature relationship. *Geochim. Cosmochim. Acta* **197**, 104–131,
616 https://doi.org/10.1016/j.gca.2016.10.010, 2017.
617 Kim, S. T. & O'Neil, J. R.: Equilibrium and nonequilibrium oxygen isotope effects in synthetic
618 carbonates. *Geochim. Cosmochim. Acta* **61**, 3461–3475, https://doi.org/10.1016/S0016-
619 7037(97)00169-5, 1997.
620 Kluge, T., Affek, H. P., Dublyansky, Y. & Spötl, C.: Devils Hole paleotemperatures and implications for
621 oxygen isotope equilibrium fractionation. *Earth Planet. Sci. Lett.* **400**, 251-260,
622 https://doi.org/10.1016/j.epsl.2014.05.047, 2014.
623 Krajewska, B. Ureases I. Functional, catalytic and kinetic properties: A review. *J. Mol. Catal.kel B:*
624 *Enzymatic*, **59**, 9-21, https://doi.org/10.1016/j.molcatb.2009.01.003, 2009.
625 Krebs, H. A., & Roughton, F. J. W. Carbonic anhydrase as a tool in studying the mechanism of reactions
626 involving H_2CO_3, CO_2 or HCO_3^-. *Biochem. J.*, **43**, 550, https://doi.org/10.1042/bj0430550, 1948.
627 Létolle, R., Gegout, P., Gaveau, B. & Moranville-Regourd, M.: Isotope fractionation of 18O during
628 precipitation of carbonates at very high pH. *C. R. Acad. Sci. II* **310**, 547–552, 1990b.
629 Liu, Y. W., Eagle, R. A., Aciego, S. M., Gilmore, R. E. & Ries, J. B.: A coastal coccolithophore
630 maintains pH homeostasis and switches carbon sources in response to ocean acidification. *Nat.*
631 *Commun*. **9**, 2857, https://doi.org/10.1038/s41467-018-04463-7, 2018.
632 Loyd, S. J. Sample, J., Tripati, R. E., Defliese, W. F., Brooks, K., Hovland, Torres M., Marlow, J.,
633 Hancock, L.G., Martin, R. & Lyons, T.: Methane seep carbonates yield clumped isotope signatures
634 out of equilibrium with formation temperatures. *Nat. Commun.* **7**, 12274,
635 https://doi.org/10.1038/ncomms12274, 2016.

636 Mangenot, X., Bonifacie, M., Gasparrini, M., Götz, A., Chaduteau, C., Ader, M., & Rouchon, V.:
637 Coupling Δ_{47} and fluid inclusion thermometry on carbonate cements to precisely reconstruct the
638 temperature, salinity and $\delta^{18}O$ of paleo-groundwater in sedimentary basins. *Chem. Geol.* **472**, 44–
639 57, https://doi.org/10.1016/j.chemgeo.2017.10.011, 2017.
640 Mangenot X., Gasparrini M., Rouchon V., Bonifacie M. Basin-scale thermal and fluid-flow histories
641 revealed by clumped isotope (D47) - Middle Jurassic reservoirs of the Paris Basin. *Sedimentology*
642 **65**, 123-150. DOI: 10.1111/sed.12427, (2018a).
643 Mangenot X., Gerdes A., Gasparrini M., Bonifacie M., Rouchon V. An emerging thermo-chronometer
644 for carbonate-bearing rocks : Δ47/(U-Pb). *Geology* **46**, 1067-1070. Doi:10.1130/G45196.1, (2018b).
645 Matsuzaki, Y. Yamada, H., Chowdhury, F. A., Higashii, T., Kazama, S., & Onoda, M.: Ab initio study
646 of CO_2 capture mechanisms in monoethanolamine aqueous solution: reaction pathways from
647 carbamate to bicarbonate. *Energy Procedia* **37**, 400–406,
648 https://doi.org/10.1016/j.egypro.2013.05.124, 2013.
649 Milliman, J. D.: Production and accumulation of calcium carbonate in the ocean: budget of a nonsteady
650 state. *Global Biogeochemical Cycles*, **7**, 927-957, https://doi.org/10.1029/93GB02524, 1993.
651 Millo, C. Dupraz, S., Ader, M., Guyot, F., Thaler, C., Foy, E., & Ménez, B.: Carbon isotope
652 fractionation during calcium carbonate precipitation induced by ureolytic bacteria. *Geochim.*
653 *Cosmochim. Acta* **98**, 107–124, https://doi.org/10.1016/j.gca.2012.08.029, 2012.
654 Mobley, H. L., & Hausinger, R. P.. Microbial ureases: significance, regulation, and molecular
655 characterization. *Microbiol. Mol. Biol. R.*, **53**, 85-108, 1989.
656 Outka, D. E., & Williams, D. C.: Sequential coccolith morphogenesis in *Hymenomonas carterae*. *J.*
657 *Protozool.* **18**, 285–297, https://doi.org/10.1111/j.1550-7408.1971.tb03319.x, 1971.

Rollion-Bard, C., Chaussidon, M. & France-Lanord, C.: pH control on oxygen isotopic composition of symbiotic corals. *Earth Planet. Sci. Lett.* **215**, 275–288, https://doi.org/10.1016/S0012-821X(03)00391-1, 2003.

Saenger, C. Affek, H. P., Felis, T., Thiagarajan, N., Lough, J. M., & Holcomb, M.: Carbonate clumped isotope variability in shallow water corals: Temperature dependence and growth-related vital effects. *Geochim. Cosmochim. Acta* **99**, 224–242, https://doi.org/10.1016/j.gca.2012.09.035, 2012.

Schauer A. J., Kelson J. R., Saenger C. and Huntington K. W. Choice of 17O correction affects clumped isotope (D47) values of CO2 measured with mass spectrometry. *Rapid Commun. Mass Spectrom.* **30**, 2607–2616, doi: 10.1002/rcm.7743, 2016.

Spooner, P. T. Guo, W., Robinson, L. F., Thiagarajan, N., Hendry, K. R., Rosenheim, B. E., & Leng, M. J.: Clumped isotope composition of cold-water corals: A role for vital effects?. *Geochim. Cosmochim. Acta* **179**, 123–141, https://doi.org/10.1016/j.gca.2016.01.023, 2016.

Staudigel, P. T., & Swart, P. K.: A kinetic difference between ^{12}C-and ^{13}C-bound oxygen exchange rates results in decoupled $\delta^{18}O$ and Δ_{47} values of equilibrating DIC solutions. *Geochem. Geophys. Geosystems* **19**, 2371–2383, https://doi.org/10.1029/2018GC007500, 2018.

Tang, J., Dietzel, M., Fernandez, A., Tripati, A. K. & Rosenheim, B. E.: Evaluation of kinetic effects on clumped isotope fractionation (Δ_{47}) during inorganic calcite precipitation. *Geochim. Cosmochim. Acta* **134**, 120–136, https://doi.org/10.1016/j.gca.2014.03.005, 2014.

Thaler, C. Millo, C., Ader, M., Chaduteau, C., Guyot, F., & Ménez, B.: Disequilibrium $\delta^{18}O$ values in microbial carbonates as a tracer of metabolic production of dissolved inorganic carbon. *Geochim. Cosmochim. Acta* **199**, 112–129, https://doi.org/10.1016/j.gca.2016.10.051, 2017.

679 Thiagarajan, N., Adkins, J. & Eiler, J.: Carbonate clumped isotope thermometry of deep-sea corals and
680 implications for vital effects. *Geochim. Cosmochim. Acta* **75**, 4416-4425,
681 https://doi.org/10.1016/j.gca.2011.05.004, 2011.
682 Tripati, A. K., Hill, P. S., Eagle, R. A., Mosenfelder, J. L., Tang, J., Schauble, E. A., Eiler, J. M.,
683 Zeebee, R. E., Uchikawa, J., Coplen, T. B., Ries, J. B. & Drew, H.: Beyond temperature: Clumped
684 isotope signatures in dissolved inorganic carbon species and the influence of solution chemistry on
685 carbonate mineral composition. *Geochim. Cosmochim. Acta* **166**, 344–371,
686 https://doi.org/10.1016/j.gca.2015.06.021, 2015.
687 Urey, H. C., Lowenstam, H. A., Epstein, S. & McKinney, C.R. Measurement of paleotemperatures and
688 temperatures of the Upper Cretaceous of England, Denmark, and the south-eastern United States.
689 *Geol. Soc. Am. Bull.* **62**, 399–416, https://doi.org/10.1130/0016-
690 7606(1951)62[399:MOPATO]2.0.CO;2, 1951.
691 Usdowski, E., Michaelis, J., Bottcher, M. E. & Hoefs, J.: Factors for the oxygen isotope equilibrium
692 fractionation between aqueous and gaseous CO_2, carbonic-acid, bicarbonate, carbonate, and water
693 (19 °C). *Z. Phys. Chem.* **170**, 237–249, 1991.
694 Watkins, J. M., Nielsen, L. C., Ryerson, F. J. & DePaolo, D. J.: The influence of kinetics on the oxygen
695 isotope composition of calcium carbonate. *Earth Planet. Sci. Lett.* **375**, 349–360,
696 https://doi.org/10.1016/j.epsl.2013.05.054, 2013.
697 Watkins, J. M. & Hunt, J. D.: A process-based model for non-equilibrium clumped isotope effects in
698 carbonates. *Earth Planet. Sci. Lett.* **432**, 152–165, https://doi.org/10.1016/j.epsl.2015.09.042, 2015.
699 Zeebe, R. E. & Wolf-Gladrow, D.: *CO_2 in Seawater: Equilibrium, Kinetics, Isotopes*. Elsevier
700 Oceanography Book Series,. **v. 65**. 346 pp. 2001
701
702 **Figures & Figure Legends**

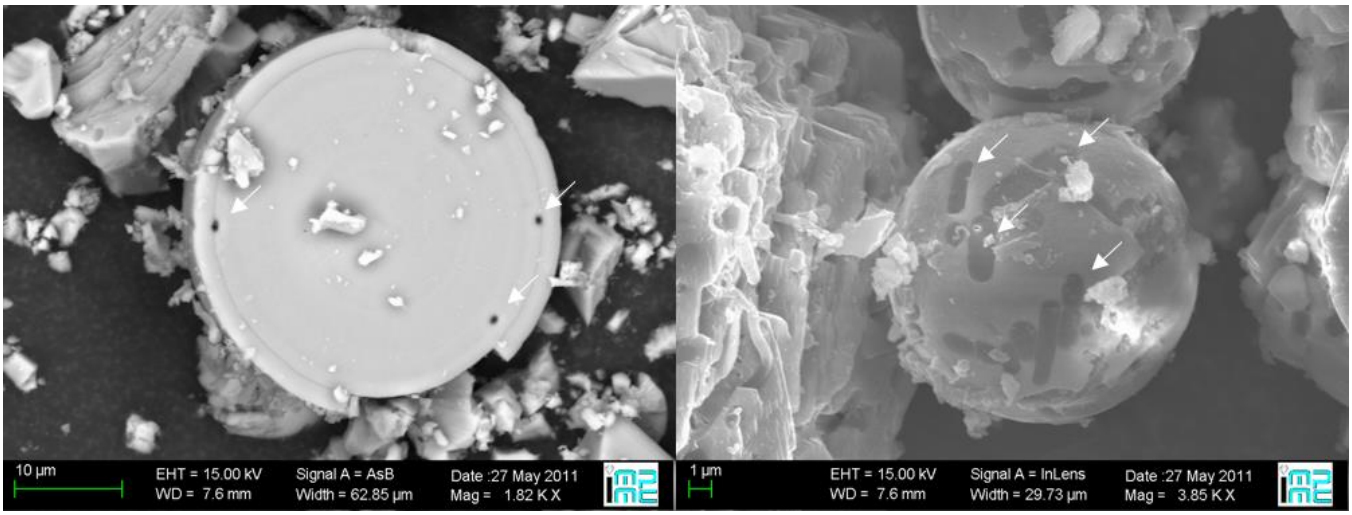

Figure 1 | Scanning electron microscopy images of the bio-induced carbonates formed with CA (almost pure calcite and traces of vaterite and aragonite as determined using X-ray diffraction (Thaler et al., 2017). The fingerprintings of *Sporosarcina pasteurii* cells are visible as black holes (on the left picture showing a cross-section of carbonate) or as rods and indicated by white arrows.

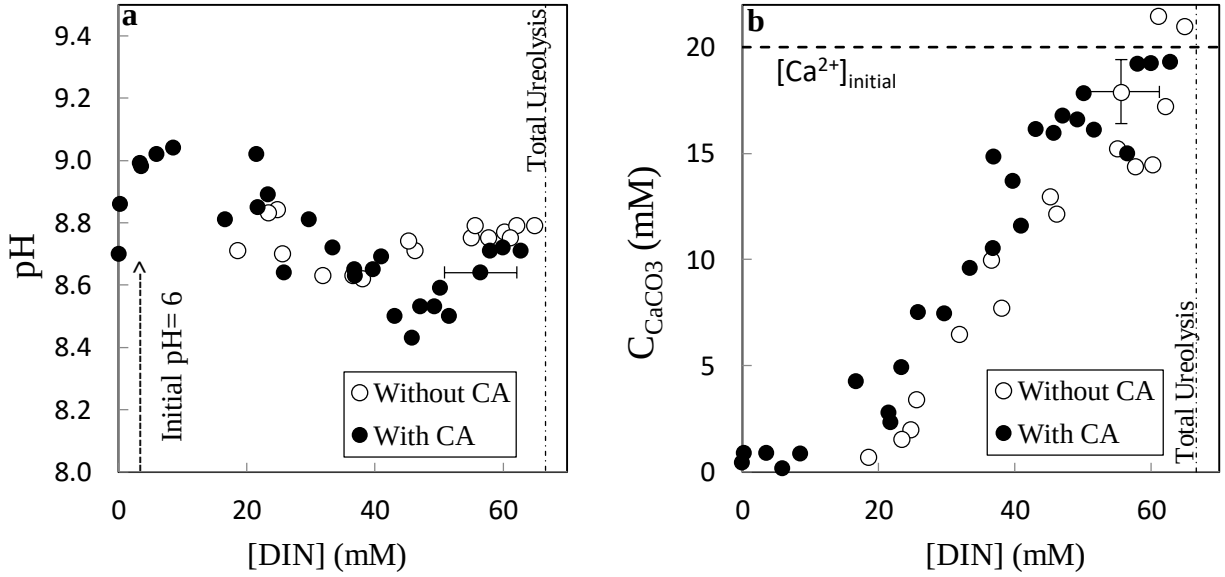

Figure 2 | Evolution of pH (**a**) and amount of precipitated calcium carbonate C_{CaCO3} (**b**) as a function of the production of dissolved inorganic nitrogen DIN (DIN = NH_3+NH_4^+) by bacteria during ureolysis,

without carbonic anhydrase (CA) (this study) and with CA (data from ref. (15)). Error bars account for 2SD and are always smaller than symbols for pH values. The mineralogy of the carbonates precipitated with or without CA was determined by X-ray diffraction, indicating that solid carbonates are mostly composed of calcite (including up to 8% of low-Mg calcite ($Mg_{0.064}Ca_{0.936})CO_3$), vaterite (2-4%) and aragonite (1-4%) Thaler et al., 2017. The influence of mineralogy on isotopic measurements and temperature estimates is discussed in the Supplementary Discussion.

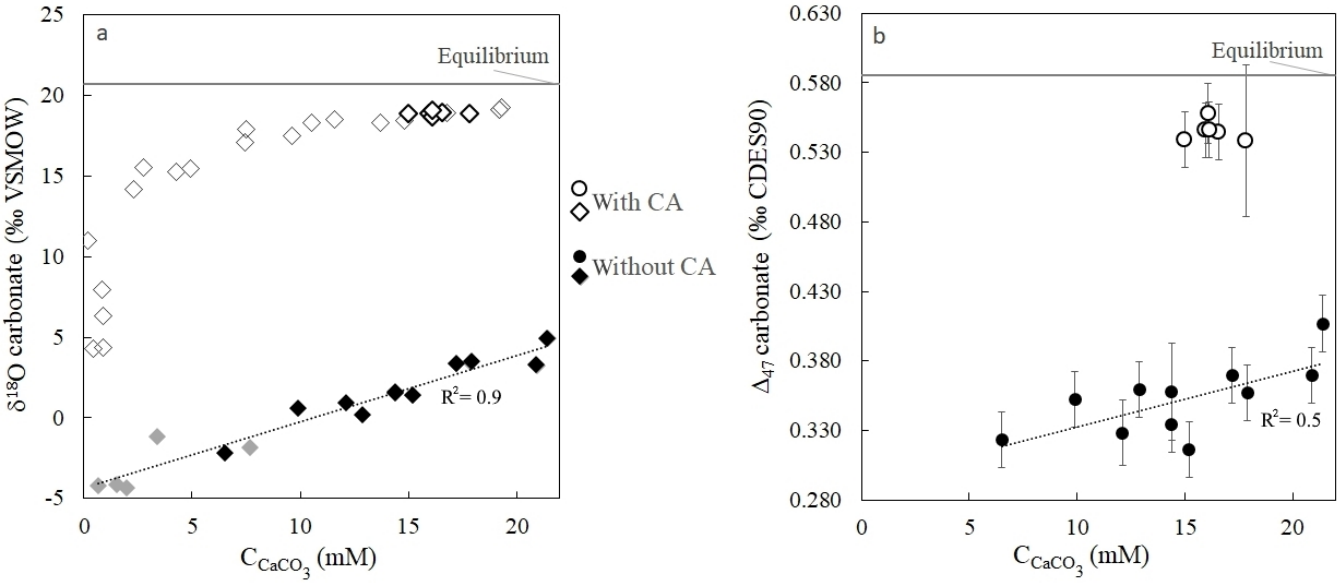

Figure 3 | Strong $\delta^{18}O$ and Δ_{47} disequilibria recorded in microbial carbonates as shown by $\delta^{18}O_{carbonate}$ (**a**) and Δ_{47} (**b**) values of calcium carbonates ($CaCO_3$) precipitated during bacterial ureolysis at 30°C (with and without carbonic anhydrase, CA; open and solid symbols, respectively) as a function of carbonate accumulation (C_{CaCO3}). Black symbols correspond to samples for which both Δ_{47} and $\delta^{18}O$ measurements were performed. The grey horizontal lines are equilibrium $\delta^{18}O_{carbonate}$ and Δ_{47} values at 30°C for calcite following Bonifacie et al., (2017) and Kim and O'Neil, (1997) calibrations, respectively. Uncertainties (one standard deviation, 1SD) are smaller than symbol for $\delta^{18}O$ and C_{CaCO3} values (Supplementary Table S1). Reported Δ_{47} uncertainties are detailed in Methods and Supplementary Discussion.

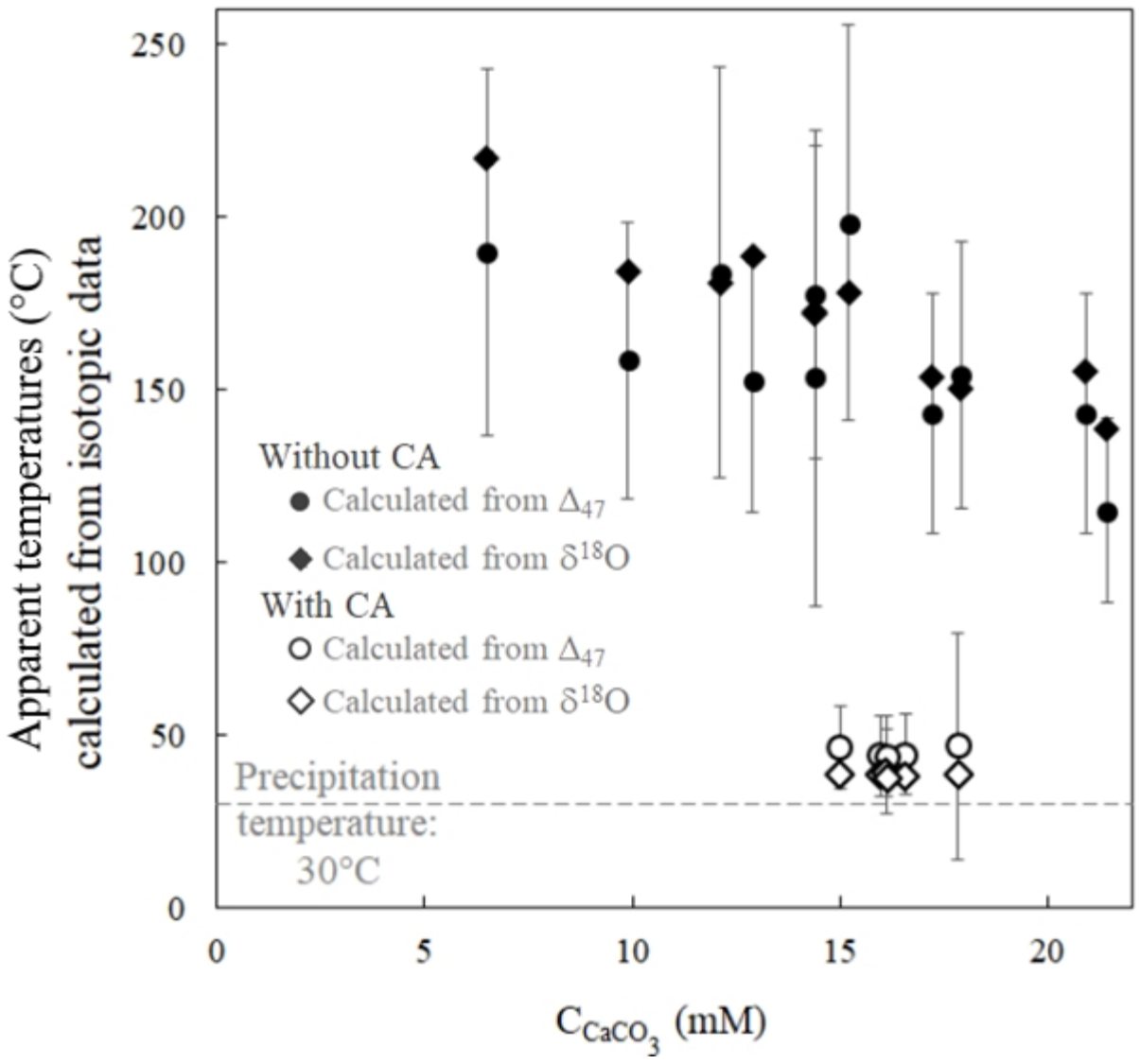

729

730 **Figure 4 | $\delta^{18}O_{carbonate}$ and Δ_{47} disequilibria in microbial carbonates induce comparable biased**
731 **estimates of precipitation temperature** as illustrated by apparent temperatures calculated from the
732 carbonate $\delta^{18}O_{carbonate}$ and Δ_{47} signatures as a function of $CaCO_3$ accumulation. Open and solid symbols
733 refer to the experiments with and without CA, respectively. The dashed grey line corresponds to the actual
734 precipitation temperature. Apparent temperatures are respectively calculated from the $\delta^{18}O_{carbonate}$ and Δ_{47}
735 calibrations to temperature of Bonifacie et al., (2017) and Kim and O'Neil, (1997). Reported uncertainties
736 were calculated as the propagation of the one standard deviation (1SD) error of the isotopic data in the
737 calibration equations (Supplementary Information).

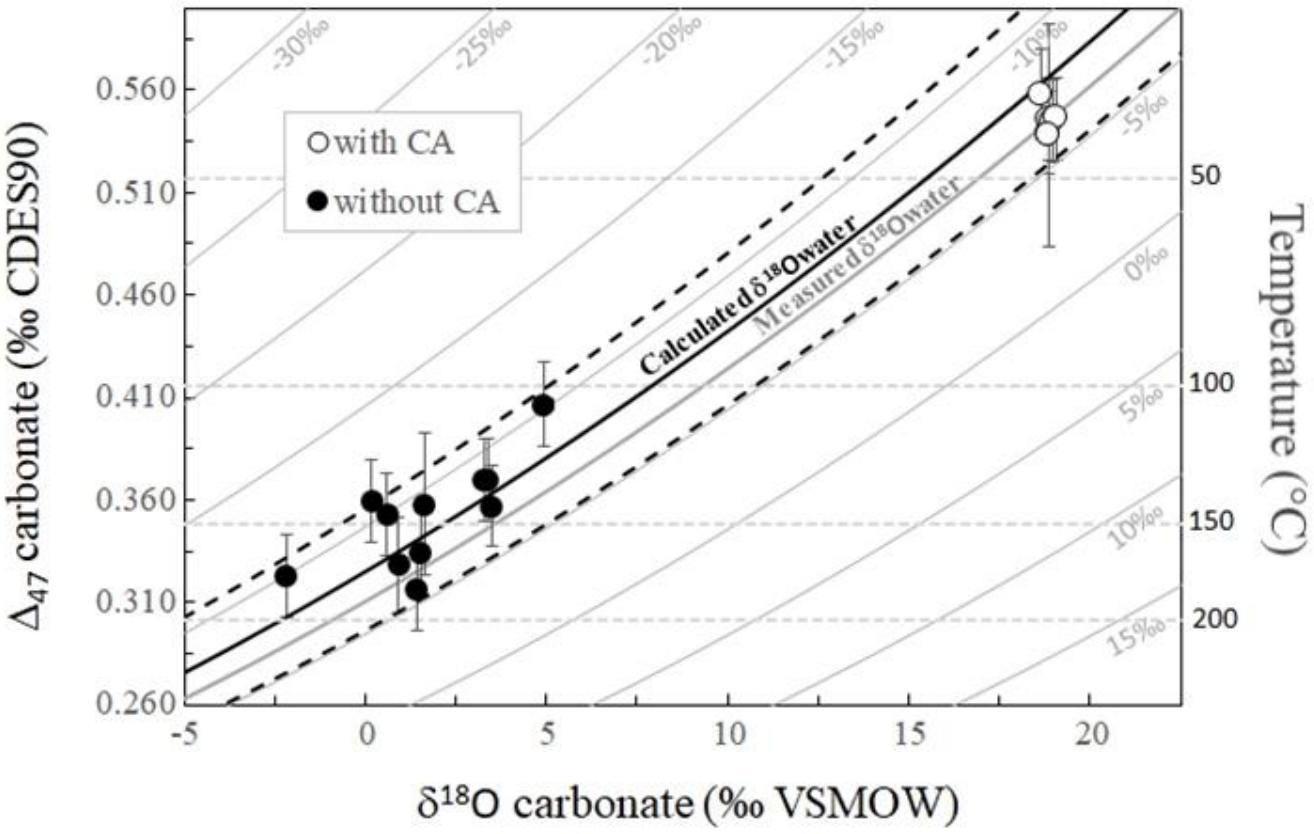

Figure 5 | Combined $\delta^{18}O_{carbonate}$ and Δ_{47} disequilibria of microbial carbonates precipitated at 30°C allow reconstruction of the $\delta^{18}O$ of the water ($\delta^{18}O_{water}$) in which they precipitate. Solid grey curves represent the calculated Δ_{47} and $\delta^{18}O_{carbonate}$ compositions of carbonates precipitated at oxygen isotope equilibrium from water with fixed $\delta^{18}O_{water}$ values (indicated on each curve) and variable temperatures. Horizontal dashed grey lines are calculated for fixed temperatures and variable $\delta^{18}O_{water}$. The average $\delta^{18}O_{water}$ value of -6.6±0.4‰ measured in our experiments is reported using the thick solid grey curve. The solid black curve was obtained using the $\delta^{18}O_{water}$ calculated with Eq. 1 (-8.0±2.8‰) with its associated errors (dashed black curves).

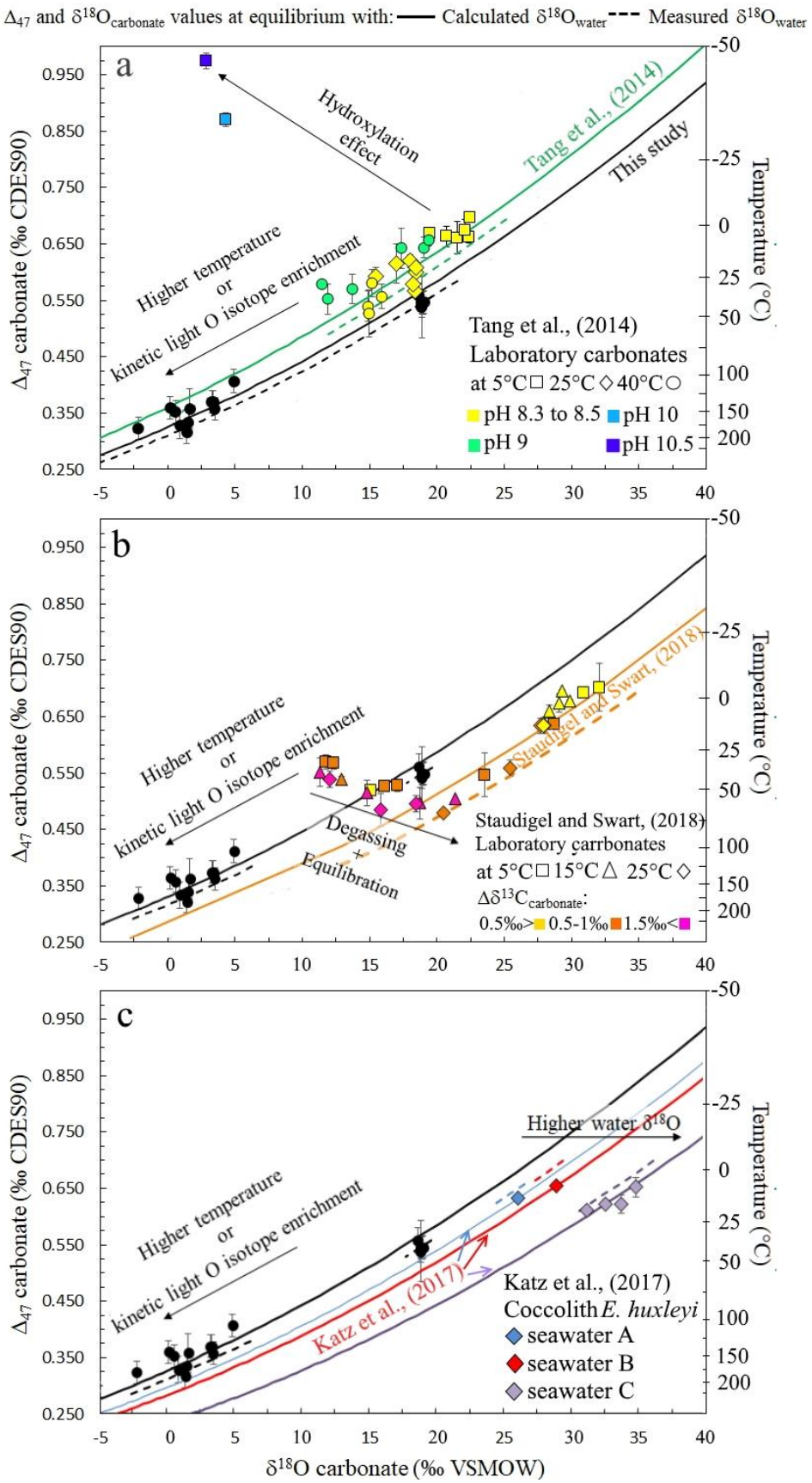
Δ47 and δ18Ocarbonate values at equilibrium with: Calculated δ18Owater Measured δ18Owater
a
Hydroxylation effect
Tang et al., (2014)
This study
Higher temperature or kinetic light O isotope enrichment
Tang et al., (2014)
Laboratory carbonates
at 5°C□ 25°C◇ 40°C○
pH 8.3 to 8.5
pH 10
pH 9
pH 10.5
b
Higher temperature or kinetic light O isotope enrichment
Degassing + Equilibration
Staudigel and Swart, (2018)
Staudigel and Swart, (2018)
Laboratory carbonates
at 5°C□ 15°C△ 25°C◇
Δδ13Ccarbonate:
0.5‰> 0.5-1‰ 1.5‰<
c
Higher water δ18O
Higher temperature or kinetic light O isotope enrichment
Katz et al., (2017)
Katz et al., (2017)
Coccolith E. huxleyi
seawater A
seawater B
seawater C
Δ47 carbonate (‰ CDES90)
Temperature (°C)
δ18O carbonate (‰ VSMOW)

750

Figure 6 | Δ_{47} and $\delta^{18}O_{carbonate}$ relationship to precipitation water $\delta^{18}O_{water}$ for other solid carbonates presenting oxygen isotope disequilibria. In (**a**) to (**c**) black data series (this study, performed at 30°C) shows how kinetic oxygen isotope fractionation in the DIC prior to carbonate precipitation can be mistaking for high temperature isotopic equilibrium. Similarly to Fig. 3, the solid curves were obtained using the $\delta^{18}O_{water}$ calculated with Eq. 1. (**a**) Abiotic carbonates from Tang et al., (2014) illustrating the effect of CO_2 hydroxylation on Δ_{47} and $\delta^{18}O_{carbonate}$ values (various pH plotted with different colors, various temperatures plotted with different symbols). (**b**) Abiotic carbonates from Staudigel and Swart, (2019) illustrating the effect of CO_2 degassing and DIC oxygen isotope equilibration with water on Δ_{47} and $\delta^{18}O_{carbonate}$ values. $\Delta\delta^{13}C_{carbonate}$ stands for the difference between the $\delta^{13}C$ value measured in carbonates and the final $\delta^{13}C$ of the data series at the end of equilibration (various $\Delta\delta^{13}C$ ranges plotted with different colors, various temperatures plotted with different symbols). (**c**) Coccolithophorid *E. huxleyi* grown at 7, 10, 15, 20 and 25°C from Katz et al., (2017) showing how coccoliths with equilibrium Δ_{47} values record the equilibrium $\delta^{18}O_{water}$ of their body water, which differs from that of the culture medium (*i.e.* artificial seawaters A, B, and C plotted with different colors).

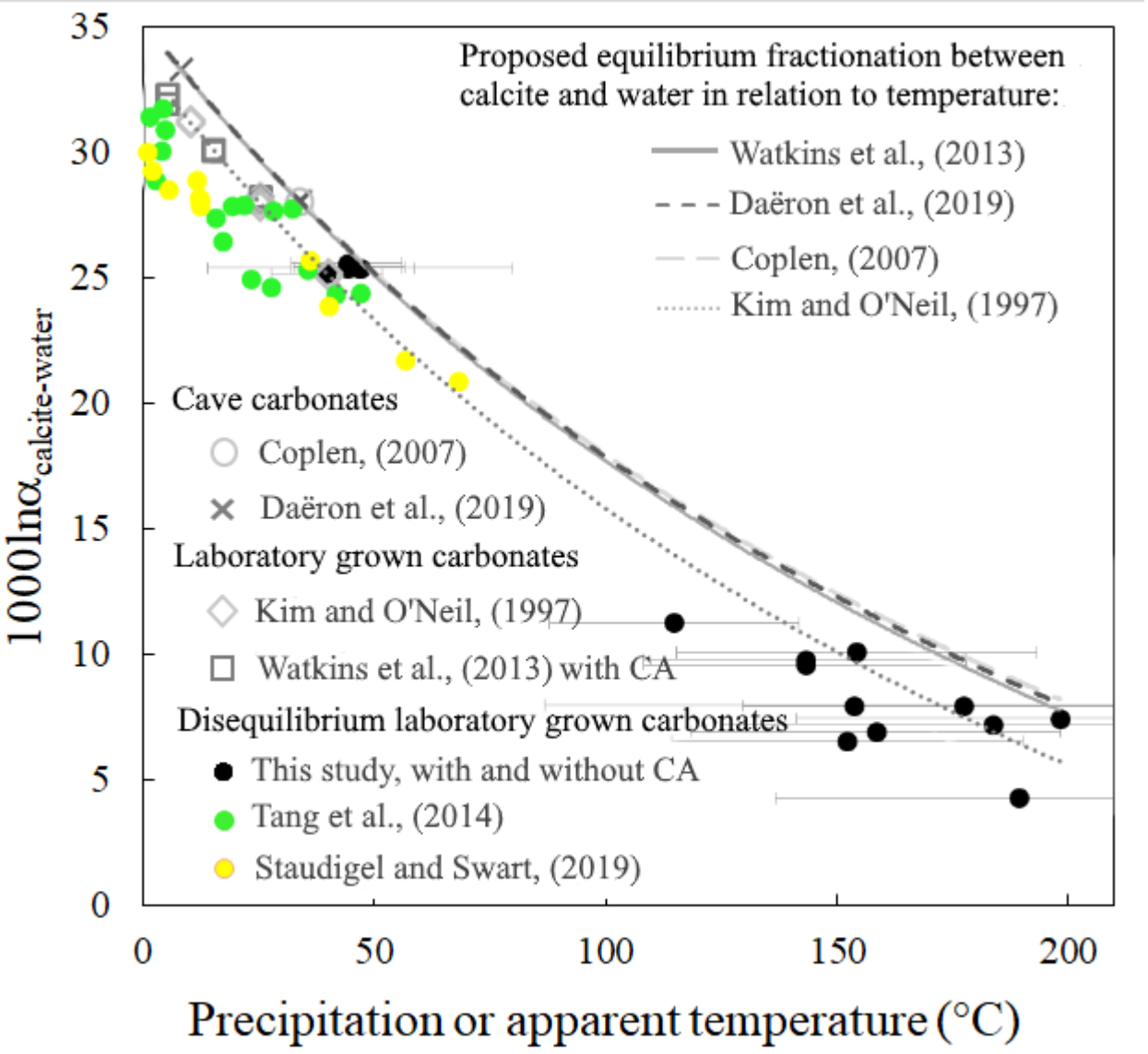

Figure 7 | The relation to temperature of equilibrium oxygen isotope fractionation factor between calcium carbonate and water ($1000\ln\alpha_{calcite\text{-}water}$) appears to be retrievable from solid carbonates (mainly calcites) in strong clumped and oxygen isotope disequilibrium such as our microbial carbonates (black dots, precipitated at 30°C) and two additional data series of laboratory grown carbonates showing disequilibrium fractionation (Tang et al., 2014; Staudigel and Swart, 2019) (green and yellow dots, respectively). The data points affected by CO_2 hydroxylation (Tang et al., 2014) or CO_2 degassing (Staudigel and Swart, 2019) (see Fig.6) are not included. Grey symbols correspond to cave carbonates precipitated at or near equilibrium (Coplen, 2007; Daëron et al., 2019) or laboratory experiments (Kim and O'Neil, 1997; Watkins et al., 2013). Those grey data series are usually considered as representative of the

777 equilibrium fractionation factor between calcium carbonate and water whose relations to temperature,
778 extrapolated at high temperature, are illustrated by the different dashed curves. Plotted temperatures
779 corresponds to precipitation temperatures except for disequilibrium carbonates for which apparent
780 temperatures have been calculated based on Δ_{47} values. X-axis errors for this study are included in the
781 symbol size. The Y-axis error for all the reconstructed temperature is given on the figure.